Time-of-Flight Photon Spectroscopy: A Simple Scheme To Monitor Simultaneously Spectral and Temporal Fluctuations of Emission on Single Nanoparticles

ARTICLE *in* ACS NANO · NOVEMBER 2012

Impact Factor: 12.88 · DOI: 10.1021/nn304842c · Source: PubMed

4 AUTHORS, INCLUDING:

Matthieu Loumaigne
University of Angers
14 PUBLICATIONS **98** CITATIONS

SEE PROFILE

ARTICLE

Time-of-Flight Photon Spectroscopy: A Simple Scheme To Monitor Simultaneously Spectral and Temporal Fluctuations of Emission on Single Nanoparticles

Matthieu Loumaigne,[†,*] Priya Vasanthakumar,[‡,§] Alain Richard,[‡] and Anne Débarre[‡,*]

[†]FemtoNanoOptics Group, LASIM, Université Lyon 1-CNRS, 43 Boulevard du 11 Novembre, 69622 Villeurbanne, France, [‡]Laboratoire Aimé Cotton, CNRS, Université Paris-Sud, Bâtiment 505, 91405 Orsay cedex, France, and [§]Dipartimento di Fisica "Enrico Fermi", Università di Pisa, Largo Bruno Pontecorvo, 3, 56127 Pisa, Italy

ABSTRACT Here we report on a novel scheme for spectral analysis that exploits the wavelength dependence of the time-of-flight of a photon in a dispersive medium. This versatile and cost-effective method, named time-of-flight photon spectroscopy (TOFPS), has the major advantage of being compatible with time-correlated single-photon counting experiments. Consequently, each photon acquired during an experiment is characterized by two parameters, its absolute time of arrival and its color, respectively. As a result, the spectral and temporal fluctuations of the emission of a single nano-object can be derived from a single measurement. As a proof of the concept, we demonstrate in the paper that the method can be used to perform Raman spectroscopy as well as fluorescence spectroscopy. We emphasize that TOFPS proves to be very efficient for improving signal-to-noise ratio in fluorescence correlation spectroscopy measurements by subsequent spectral filtering and to record luminescence spectra from single metallic particles. We demonstrate that the opportunity of simultaneously recording spectral and temporal fluctuations could be used to sort particles of different shapes inside a sample. TOFPS furthermore allows developing a new type of time interval distribution analysis which correlates the time interval between two photons and their corresponding color shift. It is applied to the analysis of the two-photon excited luminescence of a single gold nanorod. This method has a potential for a broad range of applications, among which time-resolved SERS spectroscopy and analysis of the dynamics of emission processes can be handled with new statistical approaches based on the correlation of spectral and temporal fluctuations.

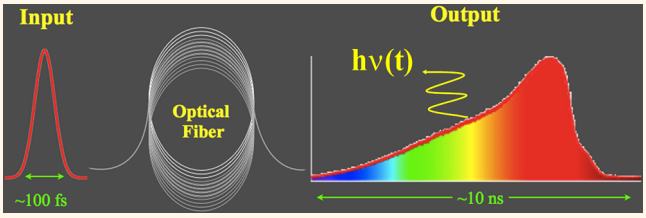

KEYWORDS: single-particle spectroscopy · time-of-flight photon spectroscopy · gold nanorod · single-particle luminescence · Raman spectroscopy · spectral fluctuations · Brownian rotation · fluorescence correlation spectroscopy

The investigation of the optical properties of individual objects of small dimensions is a rapidly growing field of research. The emission properties of many different objects have been probed, such as those of carbon nanotubes,[1] metallic particles,[2,3] and biological molecules,[4] as well as hybrid systems, including molecules and particles,[5] for example. In the following, the term object will be replaced by particle, used as a generic term to design a small object, including a molecule. The expression single-particle spectroscopy (SPS) will be used to designate the current methods shared by many optical studies on single objects. An increasing trend in the studies at the single-particle (SP) level is to develop correlated measurements of different optical properties on the same single particle. However, among the studied properties, the analysis of the spectrum of the emission is often missing. It results from the need of implementing sensitive Raman or fluorescence spectroscopy in combination with the other experimental capabilities. The main reason for the current lack of spectral analysis is the intrinsic weakness of the signal of a single particle as soon as the dimensions are in the range of some tens of nanometers or less. One issue is to get a good signal-to-noise ratio in a reasonable acquisition time, whereas the limited number of photons has

* Address correspondence to anne.debarre@u-psud.fr, matthieu.loumaigne@lasim.univ-lyon1.fr.

Received for review June 21, 2012 and accepted November 14, 2012.

Published online 10.1021/nn304842c

to be dispersed on a sufficient number of pixels of a sensitive CCD detector in order to get spectral information. The second issue, technical in nature, is the compatibility of the experimental setup with the expensive and quite large equipment needed for ultimate spectroscopic sensitivity. In fact, miniature spectrometers are now available. They prove to be very useful for analyzing large enough signals, but they presently do not cover the single-particle regime at least for small enough particles. These reasons explain the limited number of reports on SP measurements including spectroscopy, apart from dark-field spectroscopy. Dark-field spectroscopy is a very fruitful approach to both characterize the properties of shaped particles and exploit the sensitivity of the scattering response to the environment. It differs from conventional laser spectroscopy by the use of a broad-band excitation source, which makes the method quite easy to implement, avoiding tunable lasers and spectral filtering process. Yet, examples of correlated measurements on the same single particles including laser spectroscopy have demonstrated the effectiveness of Raman, SERS, and fluorescence spectroscopy to provide deep insight into the processes involved in optical responses of nanoparticles.[6−10]

The basis of SP detection is to exploit the properties of the emitted photons, which are detected one by one. The most widely used property is the time-dependent characteristics of the emission given by the arrival time of the photon. Two delays are generally recorded. One is the absolute time of arrival from the beginning of the recording process, named macrotime. The other one is the delay between the emitted photon and the corresponding excitation pulse, named microtime. The specific treatment of the huge amounts of recorded data opens the way to fruitful methods to study the dynamical properties of the emission, such as fluorescence correlation spectroscopy (FCS), molecule tracking, or lifetime measurements, for example. The second property routinely used is the polarization state of the emitted photon. It leads to polarization measurements or fluorescence anisotropy analysis, for example. The third property of the photon is its color, related to its energy. This property is used in multicolor schemes of detection, as, for example, in studies involving Förster resonant energy transfer (FRET) between a donor and an acceptor.[11] In a typical experiment, the emitted signal is split into two or more channels of detection, which include filters to select a given range of energies. The spectrum of the emission itself is generally not acquired in such experiments. Real single-molecule analysis of the spectrum has been essentially reported in Raman and surface-enhanced Raman spectroscopy (SERS) on isolated or clustered metallic particles[12,13] because of the huge enhancement of the Raman scattering of the molecule in the hot spots, which makes possible the recording of the spectrum in a limited acquisition time. The spectrum of absorption or fluorescence of single molecules in a matrix has also been successfully acquired in the pioneering experiments of Moerner and Kador[14] and Orrit and Bernard,[15] thanks to the very low temperature of the matrix.

In this paper, we report on a novel detection scheme that aims at providing the spectral response of an emission of particles, not only immobile but also diffusing in liquid, together with its temporal fluctuations with a resolution of tens of nanoseconds in a single measurement. The paper is organized as follows. In the first part of the Results and Discussion, we describe the principle of the time-of-flight photon spectroscopy method (TOFPS). In the second part of the section, we characterize the properties of the integrated spectrometer, which includes the calibration procedure, the spectral resolution, and domain. In the third part, we demonstrate the ability of the method to retrieve spectroscopic data for three different types of emission, fluorescence, Raman scattering, and luminescence. Fluorescence and Raman spectra are acquired on known systems in order to validate the TOFPS results, namely, on rhodamine B molecules in solution for the former and on DNA-wrapped single-wall carbon nanotubes dispersed in water for the latter. The last example is the luminescence spectra of metallic gold nanorods. We further demonstrate in the case of luminescence that the method allows for correlating spectral to temporal fluctuations on single particles. We show that the luminescence spectrum can be obtained simultaneously with the fluorescence correlation spectroscopy curve (FCS) of the particles. We have verified that the method is suitable to record luminescence spectra on gold particles as small as 20 nm average diameter. We then use the analogy between this method and a time-resolved spectroscopic measurement to demonstrate the example of two-photon excited luminescence (TPL) of a gold nanorod sample where the acquisition of the time of arrival and the color of any emitted photon during the same measurement allows for retrieving the spectrum of single nanorods diffusing into the sample. It paves the way for an *in situ* method of sorting different particles in a sample. In the last paragraph, we show that the simultaneous recording of spectral and temporal fluctuations on a single object, moreover, allows developing new statistical tools that could be fruitful for a better understanding of the emission itself. We discuss this possibility with the example of the two-photon luminescence of a gold nanorod. Finally, we also discuss some advantages and limitations of the method over other schemes. In the Methods section, we address the experimental techniques and the postprocessing treatment.

RESULTS AND DISCUSSION

Method. The spectral signature of an optical signal can be attained in a measurement which exploits the energy of the studied photons. Gratings and prisms convert spectral information into spatial information, which is further detected by appropriate mono- or multichannel detectors. Gratings use the well-known diffraction properties, whereas the angular dispersion of a prism exploits the variation of the refractive index of the prism material with wavelength. Alternatively, spectral information can be converted into temporal information. Such a possibility was formulated in the late 1970s.[16] The change from temporal to spectral information can be attained by the analysis of the propagation velocity dependence on the photon energy when a material with a sufficient chromatic dispersion is inserted on the path of the light beam. The method that substitutes a photon time-of-flight measurement for a spectral analysis will be further named time-of-flight photon spectroscopy (TOFPS). For almost all materials used in optics, the variation of the index of refraction with the photon energy is quite weak. In order for the time delay between two photons of different energies to be readily measured, the photon has to travel several tens of meters through the dispersive element. This challenge is solved by the use of a fiber.

Assuming first that modal dispersion can be neglected, which will be further discussed in the next subsection on the spectrometer calibration, the transit time $t(\lambda)$ of a photon into a multimode graded-index fiber of length L reads as

$$t(\lambda) = \frac{L}{v_g(\lambda)} \quad (1)$$

where v_g is the group velocity of the given photon. It is expressed as

$$v_g(\lambda) = \frac{c}{n\left(1 - \frac{\lambda}{n}\frac{dn}{d\lambda}\right)} \quad (2)$$

where n is the index of refraction of the fiber core, and c and λ are the velocity and wavelength of the photon in vacuum. By using Sellmeier's coefficients for fused silica,[17] the transit time of a $\lambda = 500$ nm photon is 260 ps shorter than that of a $\lambda = 505$ nm photon for a fiber length of 100 m. Electronics and detectors available in the early 1980s were limited to a nanosecond resolution. A time resolution on the order of 50 ps is currently available nowadays. The corresponding spectral resolution is on the order of a nanometer when $\lambda = 500$ nm.

As mentioned above, in a typical time-correlated single-photon counting (TCSPC) experiment, each photon is referenced by two characteristic times, its microtime and its macrotime. The resolution of the microtime is given by the delay between two successive pulses, 12.5 ns in the present study. The macrotime is the relevant parameter to identify temporal structures such as bursts. Here, spectral information is obtained from the microtime by means of eqs 1 and 2. As a result, each photon, initially labeled by two temporal parameters, is now labeled by the wavelength of the photon and its arrival time. The fiber acts as a spectrometer. The recording of this dual information paves the way for a number of novel applications, relying on the spectral information. A numerical post-treatment of the data, including a filtering procedure, allows retrieving the spectrum on a given temporal range, such as a burst. This method thus offers the opportunity of selecting the signal of a single nano-object among an assembly and to extract its spectrum. Reciprocally, it is possible to select a given feature in the whole spectrum and to access its dynamics with a temporal resolution of tens of nanoseconds. This can be applied to a given Raman line, for example. Moreover, one additional interest of the system is the possibility of a versatile exchange between the TOFPS setup and the classical TCSPC type of detection by simply removing the fiber.

The recorded signal, $S_r(t)$, is given by the relation

$$S_r(t) = S_{out}(t(\lambda)) \otimes E_{exc}(t) \otimes E_{em}(t) \quad (3)$$

where $S_r(t)$ is the histogram of the recorded photons with respect to the transit time. In eq 3, the symbol $\otimes$ stands for a convolution product; the time $t(\lambda)$ is deduced from eqs 1 and 2; $E_{exc}(t)$ is the temporal profile of the excitation pulse, and $E_{em}(t)$ is the temporal profile of the recorded emission signal. If the emission process corresponds to luminescence of metal particles or Raman scattering, the profile $E_{em}(t)$ is very short compared to the temporal resolution of the spectrometer and can be considered as an instantaneous pulse $\delta(t)$. On the contrary, if the emission corresponds to fluorescence, for example, the profile of $E_{em}(t)$ is more complex. It can often be fitted as an exponential decay of characteristic time τ_f with $E_{em}(t) = E_0 \exp(-t/\tau_f)$ but can also be more complex including a multiexponential decay. $S_{out}(t(\lambda))$ is the signal at the fiber output. By using eqs 1 and 2, $S_{out}(t(\lambda))$ can be expressed as a function of wavelength λ:

$$S_{out}(t(\lambda)) = (S(\lambda) \times T_{fiber}(\lambda) \times T_{exp}(\lambda)) \otimes S_{laser}(\lambda) \quad (4)$$

where $S(\lambda)$ is the investigated spectrum, $T_{fiber}(\lambda)$ is the transmission factor of the fiber, and $T_{exp}(\lambda)$ is the overall factor of transmission of the experiment that accounts for possible filters and for the spectral response of the detector. All of the factors that play a role in the signal are either known (*i.e.*, $E_{em}(t)$, $S_{laser}(\lambda)$) or can be quite easily determined in a calibration procedure, as shown below.

Spectrometer Calibration. In order to measure the time delay for different wavelengths in the optical fiber, one needs a pulsed, tunable, and polychromatic light

source. A convenient solution is to use a pulsed continuum generated by a microstructured fiber illuminated by femtosecond laser pulses and to select given wavelengths with narrow band-pass interferometric filters inside the broad-band spectrum. Here, in order to calibrate the fiber over the whole visible range, we have used three different tunable pulsed sources: the IR and frequency-doubled laser pulses of the Ti:sapphire laser and the two-photon excited luminescence (TPL) of gold nanorods. TPL is a process that is instantaneous compared to the pulse duration and which repetition rate is the same as that of the laser. The direct and frequency-doubled Ti:sapphire pulses were used to calibrate the 700−900 nm and 400−470 nm domains, respectively. TPL pulses have a very broad spectrum, which can be filtered with narrow band-pass filters. The resulting TPL-filtered pulses were used to calibrate the 470−700 nm range, which is the left blind domain.

The experimental curve obtained with the silica multimode graded-index fiber is shown in Figure 1. It is very well fitted by eqs 1 and 2 with the only free parameter L. The value of L derived from the fit is 94 m, which is in close agreement with the experimental value obtained by splitting a pulsed signal into the two channels of a fiber coupler with the long fiber in one arm and then measuring the delay. It is important to note that the curve is fitted only taking into account the chromatic dispersion. The calibration thus confirms that the hypothesis of a negligible modal dispersion used in the above model is valid, thanks to the gradient index of the fiber core. In other words, for this type of fiber, it is not necessary to calibrate each fiber. The only important parameter is the knowledge of its length. When the length is known, one can use eqs 1 and 2 to directly convert time delay into wavelength.

Spectral Resolution. Several parameters play a role in the spectral resolution. The first one is the length of the fiber, L. The longer the length is, the larger the delay is. The resolution can be increased by lengthening the fiber. Nevertheless, the delay τ_e between two successive excitation pulses creates a threshold. If the delay τ between the excitation pulse and the emitted one is longer than τ_e, part of the spectral profile will be folded up. As a result, the choice of the excitation source plays a role in the final resolution. For a source with 80 MHz repetition rate, τ_e is 12.5 ns. It is the delay obtained between two photons at 450 and 1000 nm for a fiber of length 100 m. If the resolution has to be further increased by lengthening the fiber, then the repetition rate of the source has to be reduced. A pulse picker can be useful. Nevertheless, reducing the repetition rate also reduces the rate of the emitted photons with the consequence of increasing the acquisition time to attain the same signal-to-noise ratio. The spectral resolution also depends on the temporal $E_{exc}(t)$ and spectral $S(\lambda)$ profiles of the excitation pulse, which are linked by an uncertainty relation. A broad $S(\lambda)$ spectrum limits the resolution in the case of elastic scattering or in the case of any emission whose spectrum is composed of thin lines, as in Raman scattering, for example. On the contrary, pulse duration longer than the delay to be measured limits the resolution through the $E_{exc}(t)$ term. The pulsed diode lasers are well suited to perform Raman spectroscopy. Pulse duration of 10 ps allows obtaining a spectral resolution of the order of 0.1 nm. The femtosecond sources with a repetition rate of 80 MHz are well suited to study processes that are fast compared to the spectrometer resolution when the emission spectrum does not depend on the spectral width of the excitation laser pulse.

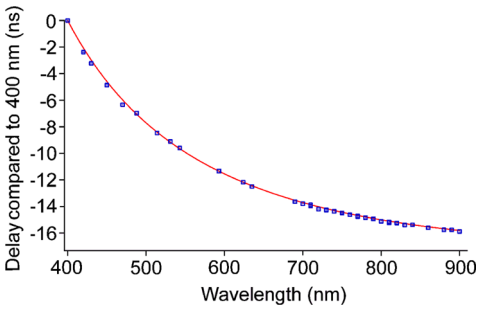

Figure 1. Calibration of the TOFPS spectrometer. The curve displays the delay between a photon of given wavelength in the range of 400−900 nm and a photon at 400 nm; squares, experiment; line, fit according to eqs 1 and 2.

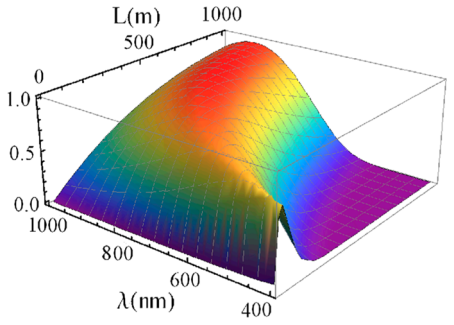

Figure 2. Figure-of-merit of the spectrometer fibered with a fused-silica optical fiber. The surface plot represents the delay to absorption ratio for a spectral shift of a nanometer between two successive photons as a function of the fiber length L and the wavelength.

Spectral Domain. A silica optical fiber allows measurements in the range of 400 up to 1270 nm. The high absorption of the fiber limits the possibility of the spectrometer to wavelengths above around 400 nm, whereas the change of sign of the function $dn/d\lambda$ implies a non-1:1 correspondence above 1270 nm and makes the use of the spectrometer more complicated above this wavelength. Measurements can only be performed with a long-pass filter rejecting wavelengths below 1270 nm.

To properly characterize the properties of the spectrometer as a function of the wavelength and of the fiber length, we have calculated the figure-of-merit, as displayed in Figure 2. The figure-of-merit is defined as

the ratio of the time delay between two photons whose wavelength is separated by a nanometer to the absorption. The larger the absorption, the greater the dispersion is. As a result, a large dispersion could be attained by using a rather absorbing material, such as silica around 400 nm, for example. Nevertheless, the analysis of the curve puts into evidence an important characteristic. The dispersion increases only linearly with the length L of the fiber, whereas the absorption increases exponentially. Consequently, in order to attain a given delay between two photons of different wavelengths, it is more effective to choose a long fiber with a weaker absorption than a short fiber. For a wavelength of 1 μm, for example, for which silica is nearly transparent, the factor of merit is maximum for a very long fiber with a length of 1 km. In conclusion, a PMMA fiber that loses 30 times higher silica fibers is not suitable for the present method.

In the third part of the present section, we report on the results obtained on systems emitting different types of signals. The first two, fluorescence emission of molecules dispersed in water and Raman scattering of DNA-wrapped nanotubes also dispersed in water, are model systems studied here to validate the spectral analysis ability of the TOFPS method. The third one corresponds to the one-photon and two-photon excited luminescence of gold nanorods. For each situation, we emphasize the new opportunities opened by this detection scheme, and we describe its limitations. As explained in detail in the paragraph Method, the excitation is provided by a Ti:sapphire pulsed laser with a repetition rate of 80 MHz and pulse duration of 100 fs. The delay between two successive pulses is 12.5 ns. The laser can be frequency-doubled in order to cover the wavelength domain ranging from 400 to 520 nm on the one hand and the fundamental domain extending from 690 to 1040 nm on the other hand. The multimode graded-index fiber has a length of 94 m. It leads to a delay of 12 ns between a photon with a wavelength of 450 nm and another photon with a wavelength of 1100 nm.

Fluorescence and Raman Spectroscopy. In this paragraph, we briefly discuss the results of two experiments that are proof of concept of the method. First, we consider the case of fluorescence. This kind of emission has been chosen as representative of a class of emissions in which the emitted photon can be delayed with respect to the excitation photon by an amount largely exceeding the temporal resolution of the detection line.

The aim of the experiment is to derive the fluorescence spectrum of a species in solution. The experiment has been performed on [9-6-diethylamino-3-xanthenylidene]-diethylammonium chloride (rhodamine B) dispersed in ethylene glycol. The molecules are excited with the frequency-doubled Ti:sapphire source at 488 nm. The excitation power is maintained below the saturation threshold of rhodamine B. The signal obtained after channeling through the 94 m long fiber is detected by an avalanche photodiode whose signal feeds a single-photon counting module (see Methods).

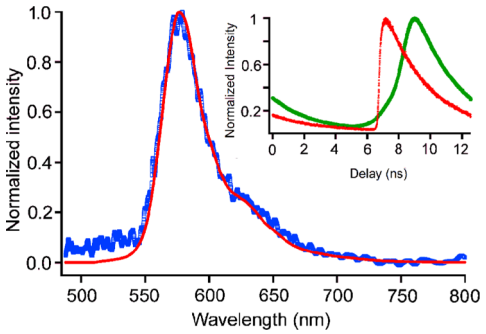

Figure 3. Fluorescence spectrum of rhodamine B molecules in ethylene glycol. Blue curve, fluorescence spectrum obtained by TOFPS after deconvolution process (see text); red curve, fluorescence spectrum obtained with a classical spectrometer; inset, green curve, raw data before deconvolution processing; red curve, independent measurement of the fluorescence decay.

In order to analyze the recorded photon stream, we first clarify the relevance of the different factors that play a role in the process, $S_{laser}(\lambda)$, $E_{exc}(t)$, and $E_m(t)$ given in eqs 3 and 4. The amplitude of the fluorescence signal depends on the intensity of the excitation, whereas the profile of emission is not very sensitive to the excitation wavelength. As a result, in a first approximation, we can consider that the fluorescence spectrum does not depend on the spectral profile of the Ti:sapphire excitation pulse. $S_{laser}(\lambda)$ can be replaced by a δ function. The duration of the excitation pulse is much shorter than the temporal resolution of the detection line, and $E_{exc}(t)$ can also be replaced by a δ function. On the contrary, the emission cannot be considered as instantaneous at the resolution scale. For a fluorescent species with a monoexponential decay, $E_m(t)$ can be expressed as $E_0\exp(-t/\tau_f)$, where τ_f is the lifetime of the molecule in the given environment. $E_m(t)$ cannot be measured directly in the TOFPS detection scheme. In fact, the main object of interest of the method is time-resolved spectral analysis, with a resolution on the order of tens of nanoseconds. For that purpose, the transit time is converted into spectral information and the information contained in this parameter is no longer available. The lifetime must be measured in a separate experiment. Nevertheless, because the power of the method rather relies on the postprocessing of the data rather than on the simple detection setup, $E_m(t)$ can be easily determined by an *in situ* measurement when the fiber is removed or alternatively by the insertion of a narrow bandwidth filter in front of the long fiber to get rid of chromatic dispersion. The fluorescence spectrum is derived from the deconvolution of $S_r(t)$ by $E_m(t)$. The result is displayed on Figure 3. In the same figure, the spectrum directly recorded with a classical spectrometer is

displayed for comparison. The agreement between the TOFPS spectrum and the spectrum acquired with the conventional spectrometer is quite satisfying, which validates the ability of the TOFPS method to perform spectral analysis of fluorescence. The profile obtained with TOFPS is noisier, essentially because the deconvolution process is very sensitive to any source of noise in the signal. In the inset of Figure 1, the fluorescence decay $E_m(t)$ obtained by inserting an efficient filter in front of the long fiber (narrow band-pass filter at 635 nm) and the raw data before deconvolution processing are displayed. The measured lifetime is 2.8 ns. This experiment has been performed as a proof of the validity of the TOFPS concept in a situation where a single exponential decay is sufficient to describe the emission decay.

The analysis could be extended to more complex situations, for which the decay is not monoexponential, at the expense of using a more sophisticated deconvolution algorithm. The inconvenience with TOFPS is the need for an independent measurement of the decay of $E_m(t)$ to recover the spectrum. Despite the existence of appropriate procedures at the expense of minor temporary changes of the setup, it can be of interest to avoid such a measurement. A possibility is to use a very long fiber (1 km) so that the lifetime of the fluorophore becomes negligible compared with the delay caused by the fiber dispersion. In such a case, the fluorescence lifetime can be neglected compared to the transit time $t(\lambda)$, and $E_{em}(t)$ can be approximated by a δ function.

By contrast, TOFPS is well suited to study the spectra of fluorophores with a short decay time or located close to metallic particles. It is well-known that the lifetime of a molecule is reduced compared to its value far from the metallic surface if the molecule is located sufficiently close to a metallic surface to undergo quenching or enhancement of fluorescence. Depending on the distance of the molecule from the metallic surface, the decay of $E_{em}(t)$ could be sufficiently shortened to become negligible compared with $t(\lambda)$ so as TOFPS could be used without any additional measurement.

The second type of emission studied is Raman scattering. Raman scattering cross section is very weak compared to fluorescence cross section, and the detection of the signal can be attained for either a concentrated sample of molecules or a small crystal or by using a surface-enhanced Raman scattering scheme when a molecule interacts with a metallic surface. Raman signatures of isolated small enough objects can nevertheless be obtained in a configuration for which the excitation is close to one of the system resonances. This condition is a prerequisite to be able to detect the spectrum of a single suspended single-wall carbon nanotube, as we have already demonstrated.[10] We have chosen to demonstrate the possibility of the TOFPS method to derive information

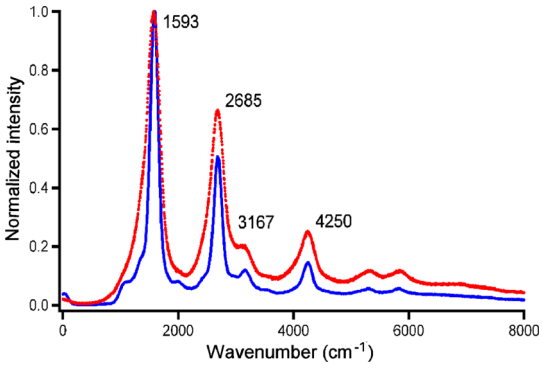

Figure 4. Raman spectrum of DNA-wrapped carbon nanotubes retrieved from a TOFPS measurement (red line). The continuous line is the measurement; the blue curve is a measurement obtained with a conventional spectrometer on the same sample.

on Raman scattering on the case of model particles diffusing in liquid, namely, DNA-wrapped single-wall carbon nanotubes dispersed in water. A huge interest has been devoted to such systems since DNA wrapping combined with size-exclusion chromatography allows sorting the different classes of nanotubes in a sample, depending on their conduction character, semiconductor or metallic, and their lengths.[18]

The TOFPS study has been performed with an excitation at 488 nm provided by the pulsed frequency-doubled Ti:sapphire laser. A reference spectrum of the nanotubes deposited on a glass substrate has been acquired in a first experiment to identify the main Raman lines (Supporting Information, Figure S1). Raman scattering is a fast emission process, at least 3 orders of magnitude faster than the response time of the setup. $E_m(t)$ can be considered as a δ function. On the contrary, the energy of the scattered photon is highly sensitive to the excitation photon energy. In fact, the relevant parameter in a Raman spectrum is not the absolute energy of the photons but their relative energy shift with respect to the excitation energy. As a result, the excitation photons of different energies produce Raman spectra shifted according to their energy. Because of the pulsed nature of the excitation, the Raman lines cannot be thinner than the width of the excitation pulse spectrum, approximately given by the inverse of the pulse duration, 100 fs in the present work. The spectrum obtained in these conditions is displayed in Figure 4. The main peak at 1593 cm^{-1} corresponds to the G-band of semiconductor nanotubes. It presents an asymmetrical shape with a bump on the left wing of the profile, corresponding to the G^--band. The peak at 2685 cm^{-1} corresponds to the G′-band.[19] Its wavenumber is up-shifted compared to the case of the reference spectrum (Supporting Information, Figure S1), in agreement with the dependence of the G′-band with respect to excitation wavelength.

The weak band at 3167 cm^{-1} can be reasonably interpreted as the residue of the H_2O Raman scattering.

The peak at ≅4250 cm^{-1} corresponds to a combination mode (1593 cm^{-1} + 2685 cm^{-1}). The very good agreement between the spectrum obtained by TOFPS and that obtained with a conventional spectrometer illustrates the ability of TOFPS to perform a spectral analysis of Raman scattering.

An exciting opportunity is then offered to explore the dynamics of a given Raman line with a temporal resolution on the order of 12.5 ns since each single detected photon labeled by its wavelength is additionally characterized by its arrival time. This could prove to be very useful in the case of SERS recording on a single particle, for example. Work is in progress in that domain. In the present case, no spectral fluctuations are expected for the Raman scattering since several nanotubes contribute to the signal. Only at resonance or pre-resonance is the Raman signal of a single nanotube sufficiently intense to be spectrally analyzed in a time compatible with its time of transit in the focal volume of the microscope. A study at the single-nanotube level supposes that the resonances are first determined, which is beyond the scope of the paper. Finally, we note that the spectral resolution, low in the case of femtosecond excitation pulses, could be greatly enhanced by using a picosecond pulsed source for the excitation.

One- and Two-Photon Excited Luminescence of Single Particles. Luminescence of noble metals was first demonstrated by Mooradian in 1969.[20] The very weak signal observed on a film is greatly enhanced in the case of particles when a resonance surface plasmon is excited. Luminescence of gold particles can be observed when electron transitions from the 5d to the 6sp bands are excited. The origin of the luminescence process is the radiative recombination of a hole−electron pair near the Fermi level.[21] The very fast emission happens in the range of 50 fs. As in the case of Raman scattering, $E_m(t)$ can be considered as a δ function. The luminescence signal is weakly sensitive to the excitation photon energy within a large range of energies suitable to excite the electron interband transitions. More precisely, the peak wavelength of the excitation pulse must be chosen in such a way that all excitation photons have a sufficient energy to be able to promote the electron transition from the 5d to the 6sp bands. If this condition is satisfied, the spectral profile of the laser can be neglected, $S(\lambda) \cong \delta$. In order to demonstrate the novel possibilities of TOFPS compared to classical spectroscopic methods, we have recorded the luminescence of gold nanorods (d = 25 nm, amine-coated, aspect ratio 2.8, Nanopartz) under one-photon pulsed excitation at 450 nm. A long-pass filter centered at 510 nm is inserted in front of the fiber to remove the excitation residue. The information on the spatial dynamics of a nano-object diffusing across the focal volume can be deduced from fluorescence correlation spectroscopy (FCS), as we have already reported for gold nanobeads.[3]

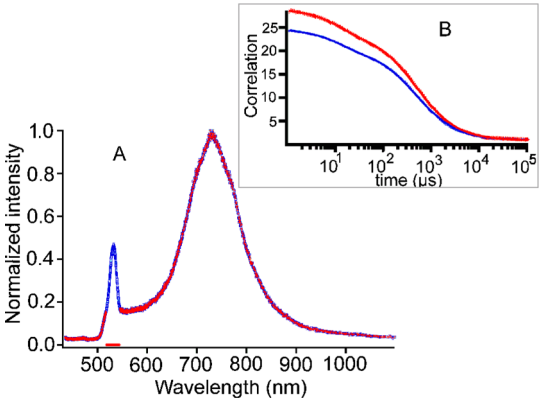

Figure 5. Luminescence spectrum of nanorods under one-photon pulsed excitation at 450 nm. (A) Spectrum retrieved from TOFPS displaying a line at around 533 nm corresponding to Raman modes of water and the luminescence profile peaking at 730 nm, normalized data. (B) Correlation curves; in blue, raw data; in red, curve obtained after filtering of the Raman contribution of water (rotation time 12 μs, diffusion time 600 μs).

Figure 5A displays the spectrum retrieved on the sample of nanorods by TOFPS. The peak located in the near-infrared domain at 730 nm corresponds to the one-photon excited luminescence emission of the nanorods at 450 nm. The first peak at 533 nm is a Raman line of water (OH vibration region). Raman scattering from solvent or a matrix is a common spurious signal in SPS. In FCS specifically, it lowers the signal-to-noise ratio, making the interpretation of the profiles less accurate. Here, this spurious signal can be easily identified by its spectrum. The TOFPS can further be used to eliminate the contribution of the corresponding Raman photons from the FCS curves by a postprocessing numerical filtering of the photons in the spectral range of 520−540 nm since these photons are also labeled by their time of arrival. The result of the filtering process is shown in Figure 5B, which displays the FCS correlation profiles of the raw data and of the data after removal of the Raman contribution. Both profiles show two components as expected. The longer component corresponds to the time of transit of the nanorod in the excited volume of the microscope, whereas the shorter one corresponds to the rotation time.[22] Its value is 12 μs. Here we have first shown that TOFPS allows retrieving both the spectrum and the corresponding FCS profile of nanorods in the same measurement. The method takes advantage of the simultaneous acquisition of the arrival time of the photon and of its wavelength, obtained with resolutions of 12.5 ns and 1 nm, respectively, in our experimental configuration. Second, the comparison between the two FCS profiles, before and after filtering (Figure 5B), demonstrates that the shape of the profile is unmodified after filtering. By contrast, the result shows an obvious enhancement of the signal-to-noise ratio. It is reported by a clear increase of the value of the correlation function at the origin $G(0)$ from 19 to 23. $G(0)$, which is inversely

proportional to the number of emissive particles simultaneously present in the excitation volume, is indeed very sensitive to noise sources, such as Raman photons, for example. The ability to obtain the spectrum at the same time as the FCS profile opens the way for efficient filtering of spurious signals, which are otherwise difficult to eliminate in the absence of a criterion to distinguish the spurious photons from the useful ones. This first demonstration suggests that, more generally, if different emitting species are mixed in a given sample, TOFPS could offer an efficient opportunity of sorting and studying the dynamics associated with each species. The post-acquisition numerical filtering can be readily adapted to synthesize optical filters, centered at chosen wavelengths with given spectral bands.

Conversely, the filtering process can be applied to the other relevant parameter, the arrival time of the photon, as described in the next experiment. We have recorded the two-photon excited luminescence of the same gold nanorods, with a pulsed excitation at a wavelength of 810 nm. A two-photon excitation configuration of the luminescence has been chosen in the following examples to demonstrate that the method is suitable for different schemes of excitation.

Since the luminescence emission corresponds to radiative plasmon de-excitation,[22,23] a burst analysis gives the opportunity to retrieve the size and shape distribution of the particles diffusing in a sample by plotting the wavelengths corresponding to the photons selected in the histogram. This is illustrated in Figure 6 for the case of two-photon excited luminescence of gold nanorods. A burst selected in the histogram (Figure 6 top) and analyzed with a shorter step displays two components (Figure 6 middle, a and b). The spectrum corresponding to these two components reveals that the two single objects that have crossed the excitation volume nearly at the same time are different. The object "a" is a square, while the shape of the object "b" is much more spherical (Figure 6 bottom). It demonstrates that the TOFPS method can be first used to numerically sort different objects inside a sample, then to retrieve the dynamics associated with a particular object of interest. It could thus avoid a complex procedure of purification, or alternatively, it could give access to the distribution of shapes in a given sample. The long plasmon resonance peak of the nanorods is very sensitive to their aspect ratio R (long axis to short axis ratio). Since the luminescence process is directly related to the emission of such plasmons, the luminescence peak should also be sensitive to R. The histogram of the peaks of luminescence obtained for the different nanorods diffusing one by one inside the observation volume should reflect the distribution of the nanorods inside the sample.

This method has two main advantages over a study of the same sample but deposited on a substrate. Neither the excitation beam nor the sample needs to be displaced during acquisition. From a technical point of view, it avoids the use of a high-resolution moving stage or of galvanometric mirrors. Second, it eliminates the heterogeneity factor related to the interaction of the particle with a non-uniform environment, the substrate on one side and water or air above the substrate.

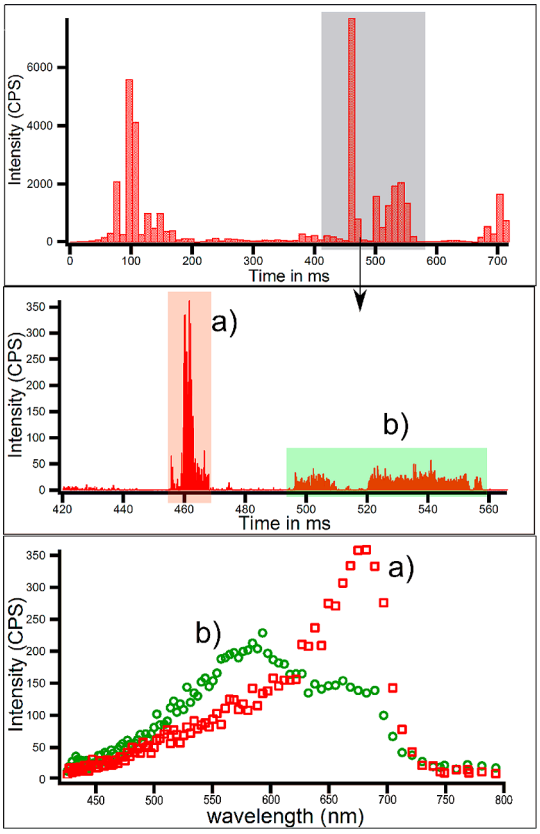

Figure 6. Histogram of the two-photon excited luminescence of the gold nanorods diffusing in water. Top: histogram with a step of 10 ms. Middle: zoom of the highlighted region of the top histogram, step 100 μs. Bottom: TOFPS spectra corresponding to the burst of region a (red squares) and to the burst of region b (green dots); pulsed excitation at 810 nm, 775 nm short-pass filter.

In the case of the study of the properties of single particles, such as luminescence as well as other scattering processes or fluorescence if the particles are functionalized with fluorophores, the TOFPS is much more sensitive than conventional spectroscopy. We have previously acquired the luminescence spectra of single gold nanoparticles in aqueous solutions.[24] Despite the low resolution of the used spectrometer, blazed in the visible range and the use of a very sensitive EMCCD camera, high signal-to-noise ratios have been obtained for quite large spherical particles with a diameter of 50 nm. Moreover, the laser power was increased to a value just below the trapping power. With the present method, it was possible to detect the luminescence of gold particles as small as 20 nm (Supporting Information, Figures S2 and S3). The increased signal-to-noise ratio directly results from the

possibility of combining the spectral analysis with the temporal resolution that allows the selection of a single burst of emission.

The strength of the dual acquisition of the time delay and of the wavelength of each single photon can be further exploited by developing new statistical approaches, in order to unravel new features of the emission of a particle. Here we will address the question of the spectral anisotropy of the two-photon excited luminescence (TPL) of gold nanorods under Brownian rotation. Briefly, if the absorption or emission dipole induced by the excitation of a particle depends on the relative orientation of the polarization and of the particle, any fluctuation of the position of the particle will result in a fluctuation of the emission. It happens in light scattering of particles of anisotropic shape,[25] and the corresponding time-dependent fluctuations are used to retrieve their rotation time in FCS experiments, for example. If, additionally, the frequency dependence of the absorption or emission probability depends as well on the relative orientation, the time-dependent fluctuations will be accompanied by correlated spectral fluctuations. Such fluctuations reflect the spectral anisotropy of the emission. Spectral fluctuations in the scattered light of particles dispersed in 80% glycerol/water mixture have been demonstrated in an elegant experiment, in which the particles are maintained in the excitation focus by 3D single-particle tracking.[26] As mentioned above, many studies have concluded that the origin of the luminescence of a gold nanoparticle results from the radiative de-excitation of the plasmons excited by the recombination of electron−hole pairs near the Fermi level.[22,23] By contrast, other reports mention the possibility of a direct recombination of the excited electron−hole pairs, enhanced by the plasmon field.[27,28] While no spectral anisotropy is expected if the first process is the dominant one, the second one would produce a spectral anisotropy in line with the anisotropy of the absorption and emission processes. We thus use the potential of the TOFPS method to address the question of the spectral anisotropy of the TPL spectrum of gold nanorods.

A possible method to study the spectral fluctuations issue is to derive the statistics of the wavelength shift between successive photons. The Brownian rotation is a stochastic process. Nevertheless, if we consider time delays sufficiently short compared to the rotation time τ_R, the probability that the delayed photon has the same color as the preceding photon should be increased compared to a random process if the emission process directly reflects the polarizability anisotropy of the particle. Figure 7 displays the histogram of the luminescence photons emitted by a two-photon excited with a step of 10 μs. The bottom trace represents the wavelength shifts of successive photons in a temporal window of 30 μs. The trace does not

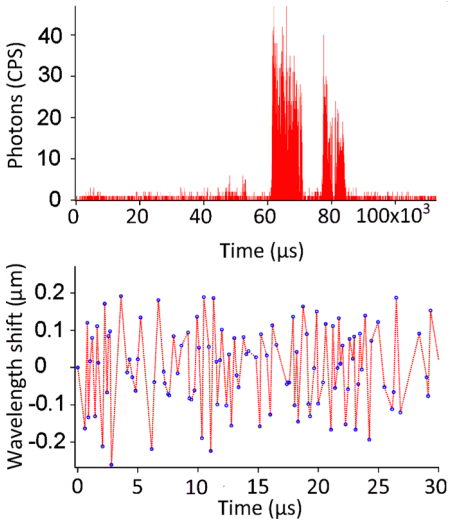

Figure 7. Spectral fluctuations of the two-photon excited luminescence of a single gold diffusing in water. Top: histogram of the luminescence photon, step 10 μs. Bottom: spectral shifts of successive luminescence photons over a period of 30 μs.

underline spectral anisotropy, which should appear as reduced fluctuations of the spectral shifts around 0. Large spectral fluctuations are observed, regardless of the time. It suggests that spectral anisotropy is not observed in this case.

We have thus realized a statistical analysis on the sample of nanorods diffusing in water one by one. The photon arrival-time interval distribution (PAID)[29] method adds to FCS information on the brightness of the diffusing objects. Here, TOFPS allows us to develop a statistical method, named color-PAID analysis by analogy to PAID analysis, and that adds information on the photon wavelength. The basic object of interest is a pair of photons, and the relevant variables are the time delay between the pairs of photons and the shift of the photon wavelengths for each pair of photons. The multi-correlation function can be displayed as a 3D plot whose x axis is the delay between the pairs of photons and the y axis the shifts between the wavelengths of the photons of the pair. The z_i variable at position (x_i,y_i) corresponds to the probability for a pair of photons of given delay x_i to have the given spectral shift y_i. For a given delay x_i, each value z_i of the probability is normalized by the total number of pairs having the delay x_i. The normalization process allows us to get rid of the temporal fluctuations. Furthermore, the maximum z_{iM} of the probabilities z_i is normalized to unity. In the example of Figure 8, which corresponds to TPL of gold nanorods, the time delay between the pairs of photons varies from 100 ns to 10 μs, by steps of 100 ns. The values of 100 ns and 10 μs have been chosen because the former is very small compared to the rotation time on the order of 12 μs, whereas the latter is on the order of the rotation time deduced from the FCS profile. The wavelength shift $\delta\lambda$ varies from −0.5 to

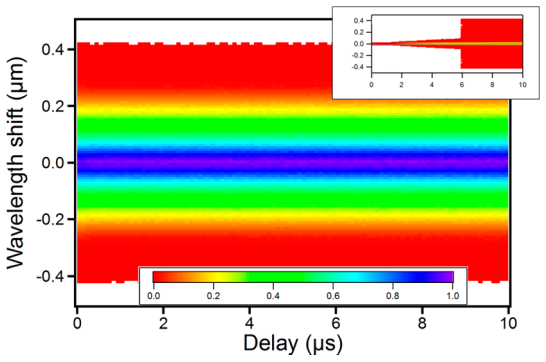

Figure 8. Three-dimensional correlation plot of spectral and temporal fluctuations for the TPL of gold nanorods (color-PAID plot). The temporal delay τ of the pairs of photons retrieved from the recorded temporal histogram is reported in abscissa. The corresponding wavelength shift $\delta\lambda$ is displayed in ordinate. The *z* value is the normalized probability that the wavelength shift of a pair of photons delayed by τ corresponds to a shift $\delta\lambda$, taken into account the number of pairs with a delay τ in the histogram of photons. The inset shows the 3D correlation plot simulated for a particle displaying spectral anisotropy under rotation.

0.5 μm by steps of 8 nm. In the inset of Figure 8, the simulated 3D plot corresponds to the case of a particle undergoing spectral anisotropy under rotation. In the simulation, the rotation time τ_R has been chosen to be 6 μs.

The comparison between the two 3D plots unambiguously demonstrates that the TPL of the nanorods does not present spectral anisotropy contrary to the case of light scattering.[26] The scattering process is a well-known elastic process, while luminescence implies more complex processes. The absence of clear signature of correlation in the color-Paid plot (Figure 8) provides an interesting indication on the TP luminescence process. It supports the idea that luminescence does not result from the direct radiative recombination of the excitons but that it results from the emission of surface plasmons that are created by the interconversion of electrons–holes.[22,23] Spectral anisotropy under rotation was not observed under TP or OP excitation scheme (Supporting Information, Figure S4). Additionally, in their work on the one-photon excited luminescence of gold nanorods, Tcherniak and co-authors[23] mention that electron–hole pairs create longitudinal surface plasmons more efficiently than transverse surface plasmons. The shape of the spectrum observed for TPL of nanorods (Figure 6 bottom) suggests that a similar result could be obtained for TPL. Additional work is needed to confirm the similarity of the one-photon and two-photon excited luminescence processes in gold nanorods.

Advantages and Limitations of TOFPS. The method allows for time-resolved spectral measurements, with a time resolution of tens of nanoseconds. The detection sensitivity is that of an avalanche photodiode (APD). The alternative to this scheme is the use of a conventional spectrometer equipped with a matrix of APD pixels as a detector. TOFPS offers several advantages compared to the latter method. First, it is very easy to implement. For example, it can be added on a time-correlated single-photon counting setup by inserting a long fiber in the detection path, in front of the detector. Second, it is a flexible setup. It is quite easy to modify the delay by increasing or decreasing the fiber length or to return to a conventional time-correlated single-photon counting scheme by removing the fiber. As a result, the resolution is readily adjustable, whereas in the case of a conventional spectrometer, a change of resolution implies a change of grating and a re-alignment of weak signals. The third important advantage is the high number of data defining each spectral profile, 4096, given by the resolution of the counting card. This number is much higher than that of an APD matrix. The fact that the acquisition of the data needs a single APD allows for strongly reducing the dark noise impact on the measurements. In fact, the dark noise of the APD is distributed over the 4096 detection channels, whereas it applies to any data point when the spectrum is acquired with an APD matrix. Finally, it is worth underlining the fact that the hybrid "fiber-numerical" spectrometer reported in this paper is "cost-effective".

The intrinsic limitation of the method compared to the use of time-resolved multichannel detectors is the lack of information on the delay between the emitted photons and the corresponding exciting pulses. The information in the spectral domain is obtained at the expense of such data. It implies that some assumptions or initial measurements have to be performed on the samples to derive lifetimes or emission decays if needed before processing the data. As mentioned above, such data can be, in most situations, quite readily retrieved through simple procedures. One is the removal of the fiber itself; another one consists of inserting an efficient filter in front of the long fiber.

CONCLUSION

In summary, we have described a new spectroscopic method based on photon time-of-flight measurements. The method offers the opportunity to record emission spectra of single nano-objects, such as gold nanorods, for example. Its high sensitivity allows performing luminescence spectroscopy on tiny particles down to 20 nm. The temporal resolution of the spectral measurements is in the nanosecond range. We have demonstrated that different types of emissions can be monitored by the method, such as one-photon or two-photon excitation luminescence, fluorescence, or Raman scattering. The experimental implementation is straightforward since it consists of inserting a fiber between the emitted signal and the detector and developing the corresponding data postprocessing. Moreover, this method paves the way for new studies. It allows for time-resolved SERS spectroscopy at the single-particle level, for example, or for studying the

FCS response of hybrid probes combining metallic particles and fluorescent molecules with a good signal-to-noise ratio. Finally, the possibility of monitoring simultaneously the spectral and temporal fluctuations of a given light emission process offers the opportunity to unravel properties of the emission by studying the possible correlation between spectral and temporal fluctuations.

METHODS

Optical Setup. The experimental setup is based on a scanning stage confocal microscope. A Ti:sapphire pulsed laser (80 MHz repetition rate, 100 fs pulse duration) is used to illuminate the sample through a water-immersion high numerical aperture objective (NA = 1.2, 60×, Nikon) after cleaning through a long-pass filter (3RD760LP, Omega). Alternatively, the IR laser can be frequency-doubled in a BBO crystal for one-photon excitation of the sample in the range of 400−520 nm. A 10/90 beamsplitter is used to reflect the laser beam toward the objective and to transmit the luminescence collected by the same objective. The beamsplitter was selected to minimize the aberrations of the focal volume. The latter is precisely monitored by a fine computer-controlled adjustment of the objective ring, optimized for a working distance of 15 μm above the interface. The signal, extended by a x2 telescope, is directed to an approximately 90 m long silica graded-index multimode optical fiber (Corning Optical Fiber, 50 μm core, NA = 0.2) after passing through a confocal pinhole of 25 μm. The numerical aperture of the beam at the entrance of the fiber is 0.09, which limits the effect of a possible modal dispersion. The fiber is connected to an avalanche photodiode (Micron Phot Device PDF series). The temporal response of the avalanche photodiodes is 50 ps. The signal is spectrally separated from the laser residue with the help of an interferometric filter (Semrock FF01-770/SP-25 or Omega 510 LP). Despite the inherent small excitation volume produced by two-photon excitation, the pinhole was maintained in the detection path to ensure that the observation volumes are equivalent in the different detection configurations. The avalanche photodiode signals are fed to a single-photon counting module (Picoquant PicoHarp 300). A home-written computer program allows for histogram analysis, temporal filtering, data correlation analysis, and microtime to wavelength conversion.

Conflict of Interest: The authors declare no competing financial interest.

Acknowledgment. The authors greatly acknowledge the financial support provided, within the European Union's FP6, by the ERANET project NanoSci-ERA: Nanoscience in the European Research Area, in the context of the MOLIMEN consortium (MOlecules and LIght in MEtal Nanostructures). The work described here has also been supported by Triangle de la physique (2007-42 NOIBIPHOT contract) and by C'Nano Ile-de-France (Biosondor contract).

Supporting Information Available: DNA-wrapped carbon nanotube Raman spectra, TOFPS of 20 nm gold particles, 3D correlation plot of spectral and temporal fluctuations for the one-photon excited luminescence of gold nanorods. This material is available free of charge *via* the Internet at http://pubs.acs.org.

REFERENCES AND NOTES

1. Sfeir, M. Y.; Beetz, T.; Wang, F.; Huang, L.; Henry Huang, X. M.; Huang, M.; Hone, J.; O'Brien, S.; Misewich, J. A.; Heinz, T. F.; *et al.* Optical Spectroscopy of Individual Single-Walled Carbon Nanotubes of Defined Chiral Structure. *Science* **2006**, *312*, 554–556.
2. Mock, J. J.; Smith, D. R.; Schultz, S. Local Refractive Index Dependence of Plasmon Resonance Spectra from Individual Nanoparticles. *Nano Lett.* **2003**, *3*, 485–491.
3. Loumaigne, M.; Richard, A.; Laverdant, J.; Nutarelli, D.; Débarre, A. Ligand-Induced Anisotropy of the Two-Photon Luminescence of Spherical Gold Particles in Solution Unraveled at the Single Particle Level. *Nano Lett.* **2010**, *10*, 2817–2824.
4. Weiss, S. Measuring Conformational Dynamics of Biomolecules by Single Molecule Fluorescence Spectroscopy. *Nat. Struct. Mol. Biol.* **2000**, *7*, 724–729.
5. Loumaigne, M.; Praho, R.; Nutarelli, D.; Werts, M. H. V.; Débarre, A. Fluorescence Correlation Spectroscopy Reveals Strong Fluorescence Quenching of FITC Adducts on PEGylated Gold Nanoparticles in Water and the Presence of Fluorescent Aggregates of Desorbed Thiolate Ligands. *Phys. Chem. Chem. Phys.* **2010**, *12*, 11004–11014.
6. Stiles, R. L.; Willets, K. A.; Sherry, L. J.; Roden, J. M.; Van Duyne, R. P. Investigating Tip−Nanoparticle Interactions in Spatially Correlated Total Internal Reflection Plasmon Spectroscopy and Atomic Force Microscopy. *J. Phys. Chem. C* **2008**, *112*, 11696–11701.
7. Haran, G. Single-Molecule Raman Spectroscopy: A Probe of Surface Dynamics and Plasmonic Fields. *Acc. Chem. Res.* **2010**, *43*, 1135–1143.
8. Qin, L.; Zou, S.; Xue, C.; Atkinson, A.; Schatz, G. C; Mirkin, C. A. Designing, Fabricating, and Imaging Raman Hot Spots. *Proc. Natl. Acad. Sci. U.S.A.* **2006**, *103*, 13300–13303.
9. Maruyama, Y.; Futamata, M. Elastic Scattering and Emission Correlated with Single-Molecule SERS. *J. Raman Spectrosc.* **2005**, *36*, 581–592.
10. Débarre, A.; Kobylko, M.; Bonnot, A.-M.; Richard, A.; Popov, V. N.; Henrard, L.; Kociak, M. Electronic and Mechanical Coupling of Carbon Nanotubes: A Tunable Resonant Raman Study of Systems with Known Structures. *Phys. Rev. Lett.* **2008**, *101*, 197403–197406.
11. Roy, R.; Hohng, S.; Ha, T. A Practical Guide to Single-Molecule FRET. *Nat. Methods* **2008**, *5*, 507–516.
12. Nie, S.; Emory, S. R. Probing Single Molecules and Single Nanoparticles by Surface-Enhanced Raman Scattering. *Science* **1997**, *275*, 1102–1106.
13. Kneipp, K.; Wang, Y.; Kneipp, H.; Perelman, L. T.; Itzkan, I.; Dasari, R. R.; Feld, M. S. Single Molecule Detection Using Surface-Enhanced Raman Scattering. *Phys. Rev. Lett.* **1997**, *78*, 1667–1670.
14. Moerner, W. E.; Kador, L. Optical Detection and Spectroscopy of Single Molecules in a Solid. *Phys. Rev. Lett.* **1989**, *62*, 2535–2538.
15. Orrit, M.; Bernard, J. Single Pentacene Molecules Detected by Fluorescence Excitation in a *p*-Terphenyl Crystal. *Phys. Rev. Lett.* **1990**, *65*, 2716–2719.
16. Whitten, W. B.; Ross, H. H. Fiber Optic Waveguides for Time-of-Flight Optical Spectrometry. *Anal. Chem.* **1979**, *51*, 417–419.
17. Maltison, I. H. Interspecimen Comparison of the Refractive Index of Fused Silica. *J. Opt. Soc. Am.* **1965**, *55*, 1205–1209.
18. Strano, M. S.; Zheng, M.; Jagota, A.; Onoa, G. B.; Heller, D. A.; Barone, P. W.; Usrey, M. L. Understanding the Nature of the DNA-Assisted Separation of Single-Walled Carbon Nanotubes Using Fluorescence and Raman Spectroscopy. *Nano Lett.* **2004**, *4*, 543–550.
19. Dresselhaus, M. S.; G. Dresselhaus, G.; Jorio, A.; Souza Filho, A. G.; Saito, R. Raman Spectroscopy on Isolated Single Wall Carbon Nanotubes. *Carbon* **2002**, *40*, 2043–2061.
20. Mooradian, A. Photoluminescence of Metals. *Phys. Rev. Lett.* **1969**, *22*, 185–187.
21. Sonnichsen, C.; Franzl, T.; Wilk, T.; von Plessen, G.; Feldmann, J.; Wilson, O.; Mulvaney, P. Drastic Reduction of Plasmon Damping in Gold Nanorods. *Phys. Rev. Lett.* **2002**, *88*, 077402–077405.

22. Varnavski, O. P.; Goodson, T.; Mohamed, M. B.; El-Sayed, M. A. Femtosecond Excitation Dynamics in Gold Nanospheres and Nanorods. *Phys. Rev. B* **2005**, *72*, 235405–235413.
23. Tcherniak, A.; Dominguez-Medina, S.; Chang, W. S.; Swanglap, P.; Slaughter, L. S.; Landes, C. F.; Link, S. One-Photon Plasmon Luminescence and Its Application to Correlation Spectroscopy as a Probe for Rotational and Translational Dynamics of Gold Nanorods. *J. Phys. Chem. C* **2011**, *115*, 15938–15949.
24. Loumaigne, M.; Vasanthakumar, P.; Richard, A.; Débarre, A. Influence of Polarization and Wavelength on Two-Photon Excited Luminescence of Single Gold Nanospheres. *Phys. Chem. Chem. Phys.* **2011**, *13*, 11597–11605.
25. Bohren, C. F.; Huffman, D. R. In *Absorption and Scattering of Light by Small Particles*; Bohren, C. F., Huffman, D. R., Eds.; Wiley-VCH: Weinheim, Germany, 2004; Chapter 5.
26. Cang, H.; Montiel, C.; Xu, S.; Yang, H. Observation of Spectral Anisotropy of Gold Nanoparticles. *J. Chem. Phys.* **2008**, *129*, 044503-1–044503-5.
27. Imura, K.; Nagahara, T.; Okamoto, H. Plasmon Mode Imaging of Single Gold Nanorods. *J. Am. Chem. Soc.* **2004**, *126*, 12730–12731.
28. Mohamed, M. B.; Volkov, V.; Link, S.; El-Sayed, M. A. The 'Lightning' Gold Nanorods: Fluorescence Enhancement of over a Million Compared to the Gold Metal. *Chem. Phys. Lett.* **2000**, *317*, 517–523.
29. Laurence, T. A.; Kapanidis, A. N.; Kong, X.; Chemla, D. S.; Weiss, S. Photon Arrival-Time Interval Distribution (PAID): A Novel Tool for Analyzing Molecular Interactions. *J. Phys. Chem. B* **2004**, *108*, 3051–3067.